The influence of an obstacle placed in the ablation plasma on the properties of oxide thin films

F. GHERENDI
National Institute for Lasers, Plasma and Radiation Physics (NILPRP), Plasma Physics and Nuclear Fusion Laboratory, L 22, P.O. Box MG-36, 077125, Magurele-Bucharest, Romania

Indium oxide and zinc oxide thin films were grown by pulsed electron beam deposition on glass, in pure oxygen at room temperature, using a 10mm width metal strip as mechanical obstacle in the path of the ablation plasma plume, placed at 17 mm from the substrate. The electrical and optical properties of these thin films grown in the shadow of the obstacle and near it were studied comparatively. The spatial profile of the resistivity across the obstacle shadow was measured using the 2 and 4 probes techniques. The In_2O_3 film has a high resistivity (~$2x10^3$ Ω·cm) in the center of the obstacle shadow, while the adjacent regions have low resistivities (~$6x10^{-4}$ Ω·cm). A smaller, but still significant increase of resistivity behind the obstacle was observed for ZnO films (~0.6 Ω·cm vs. ~$6x10^{-3}$ Ω·cm in the adjacent regions). The increase of resistivity is explained by an additional incorporation of oxygen atoms from the working gas in the film grown behind the obstacle. Optical transmission measurements showed good transparency with an increase of the absorption coefficient in the film region grown behind the obstacle, accompanied by a slight decrease of the band gap determined from the Tauc plot.

(Received October 16, 2013; accepted November 7, 2013)

Keywords: Transparent conducting oxides, Thin films, Resistivity, Shadow mask, Ablation, Pulsed electron beam deposition

1. Introduction

The control of the film properties on different regions of a substrate during a single deposition process would be an important achievement for shortening industrial processes, and could determine important cost reductions in applications.

In_2O_3 and ZnO are typical conducting oxides used for transparent electronics [1-3]. The growing interest in ZnO thin films as a replacement for indium tin oxide is due to abundance and toxicity reasons. Pulsed laser deposition (PLD) is a typical method to grow oxide thin films [4, 5]. Pulsed electron beam deposition (PED) used in this work is also an ablation method, useful for growing smoother oxide thin films and with less particulates [6].

A possible method to influence the film growth process involving ablation plasma would be the insertion of an obstacle in the plasma path to the substrate.

Experiments concerning the growth of thin films behind an obstacle were previously reported for PLD [7-9]. The presence of an obstacle in the ablation plasma plume prevents droplets from the target to reach the substrate, a known issue of the ablation deposition methods. The thickness of the film grown by PLD behind the obstacle is typically ~10-12 times lower than in the adjacent regions, depending on the obstacle size and distance from the substrate.

The PED method [6] has similarities with the PLD method [4, 10]; both deposition methods are based on the ablation of a target using a pulsed beam with comparable energies, resulting a film with the same composition as the target, but PED uses an electron beam instead of the PLD laser beam. [11]. Previous studies, without obstacle, shown that stoichiometric, dense, smooth and even epitaxial ZnO and In_2O_3 thin films can be grown by PED [12, 13] with tunable electrical and optical properties.

This work aims to investigate and compare the influence of an obstacle on the properties of the indium and zinc oxide thin films grown by PED at room temperature and on glass substrates. The changes in the electrical and optical properties of the films grown in the shadow of the obstacle were investigated in comparison with the same properties in the adjacent regions. In this purpose, a method for determining the resistivity of the film with spatial resolution by scanning the film surface with two electrical microprobes was developed. Resistivity measurements in Van der Pauw geometry and Hall effect measurements of the carriers density and mobility were also performed. The optical transmission of the films was measured in the region grown in obstacle shadow and in the adjacent regions, in order to determine the influence of the obstacle on the transparency and band gap.

2. Experimental setup

In_2O_3 and ZnO thin films were grown by PED method either on 12 x 25 mm glass substrates in the presence of a mechanical obstacle in the path of the plasma plume towards the substrate, or without obstacle on 12mm square glass substrates for performing Hall effect measurements.

The PED set-up was described in detail elsewhere [6, 13, 14]. The 100 ns pulsed electron beam is produced in a channel-spark discharge which consists of a hollow cathode and a dielectric capillary tube (6 mm diameter and 110 mm length). A grounded stainless steel vacuum

chamber containing the capillary tube, target and substrate holder is the anode for the capillary discharge. The film growth setup is sketched in figure 1. The pulsed electron beam interacts with the target at an angle of 45° and the target-substrate distance is 40 mm. The PED working pressure was $1.3x10^{-2}$ mbar oxygen, the working voltage was -14kV and the pulsed electron beam repetition rate was 1 Hz.

The obstacle was a 10 mm width metallic stripe, which was placed between the target and the substrate, at 17 mm distance from the substrate. The 12x25 mm glass substrate is positioned with the long edge (25mm) along the **x** axis.

The sheet resistance profiles across the obstacle shadow (the **x** axis in figure 1) were measured using the 2 and 4 in line microprobes methods. In order to calculate the resistivity profiles from the sheet resistance profiles, spatially resolved film thickness measurements were made by Rutherford back-scattering (RBS) and step profilometry. The electrical transport properties of the thin films (resistivity, carrier density and mobility) were measured at room temperature using a MMR Technologies Hall and Van der Pauw measurement system.

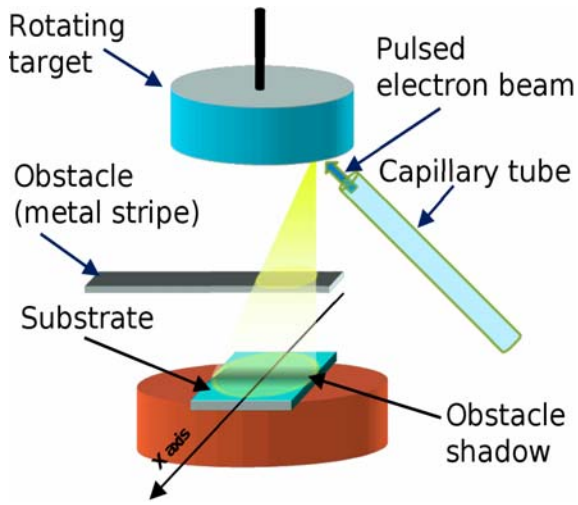

Fig.1: Experimental setup.

Electrical measurements were performed on thin films grown without obstacle at different pressures: $1.3x10^{-2}$ and $2x10^{-2}$ mbar oxygen for In_2O_3 films, and at $1.3x10^{-2}$ and $1.5x10^{-2}$ mbar oxygen in the case of ZnO films. The optical transmittance measurements of the thin films were performed with a Varian Cary 5000 spectrophotometer.

3. The two and four in line probes methods for determining the sheet resistance profile of thin films

The electrical measurements of the In_2O_3 film grown with obstacle at $1.3x10^{-2}$ mbar revealed a highly resistive central region (corresponding to the obstacle shadow) and two highly conductive wings (adjacent regions).The resistance of the film measured between the conducting wings was R_{tot}=380 MΩ. In the case of ZnO grown at $1.3x10^{-2}$ mbar, the increase of the resistance in the central region was significantly lower: R_{tot}=45 kΩ between the conducting wings.

In order to measure the sheet resistance of the film $\mathbf{R_0(x)}$ with spatial resolution, resistance measurements were performed by scanning the film surface with microprobes on the **x** direction (across the obstacle shadow, see figure 1), using 2 or 4 in line microprobes aligned perpendicularly to the scan direction.

The 4 in line microprobes method is best suitable for low resistances [15], due to the fact that, by separating the current injection probes from the sense (measure) probes, the contact resistance of the sense probes does not influence the measurement. On the other hand it is limited in the high resistance range by the voltmeter input impedance. Unlike the 4 probes method, the 2 probes method is not limited by the voltmeter input impedance, being better suited for high resistance measurements.

The expression of the total resistance of the film measured between the conductive wings in function of the sheet resistance profile is**:**

$$R_{tot} = \frac{1}{W}\int_0^L R_0(x)\cdot dx \qquad (1)$$

where **W** is the total film width, **L** is the total film length, $R_0(x)$ is the sheet resistance (in Ω/square) at the **x** position, ρ(x) and τ(x) the film resistivity and thickness respectively at the **x** position.

The theory of multiple microprobes measurement of the sheet resistance (fig. 2a) is largely treated in the literature [15, 16]. The theory is formulated for small distances between the probes [15], assuming that the sheet resistance $\mathbf{R_0}$ is approximately constant in any point **P** closer to the probes than the distance between them (figure 2a). In our measurements, the probes are placed on a line perpendicular to the **x** axis (see figure 2b) and the distances between the probes were ~1 mm.

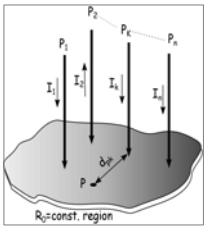

a) multiple probes

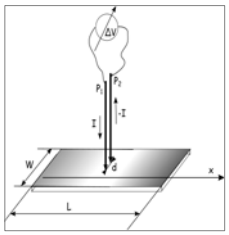

b) 2 probes

Fig. 2: Illustration of microprobes measurement on thin films.

The potential in the near vicinity of the probe noted by **k** can be evaluated using the following approximation [16]:

$$V_k = -\frac{R_0}{2\cdot\pi}\cdot\left(I_k\cdot r+\sum_{i=1,i\neq k}^{n} I_i\cdot\ln\left(d_{pi}\right)\right)+V_\infty \quad (2)$$

where **r** is the probe contact radius on the film.

Considering only 2 probes (figure 2b) which inject a current I in the film, and substituting I_1=I and I_2=-I (Kirchoff law, sum of all currents is 0) in formula (2), we obtain:

$$V_2-V_1=\frac{R_0}{2\cdot\pi}\cdot\left[2\cdot I\cdot\ln(r)-2\cdot I\cdot\ln(d)\right]= =\frac{R_0\cdot I}{\pi}\cdot\ln\left(\frac{d}{r}\right) \quad (3)$$

with **d** the distance between the probes.

We put the probes on the film at different x positions (fig. 2b), keeping constant the distance between them. Setting a constant potential difference between the probes $\Delta V=V_2-V_1$, we measure the probe current I(x). The 2 probes measured resistance in function of the position will be $R_{2p}(x)=\Delta V/I(x)$. We can calculate the sheet resistance $R_0(x)$ from (3), as a function of the 2 points resistance profile $R_{2p}(x)$:

$$R_0(x)=\frac{\Delta V}{I(x)}\cdot\frac{\pi}{\ln\left(\frac{d}{r}\right)}=R_{2p}(x)\cdot\frac{\pi}{\ln\left(\frac{d}{r}\right)} \quad (4)$$

The contact radius **r** cannot be precisely measured, but it is possible to evaluate ln(**d**/**r**) using the measured total resistance of the film $\mathbf{R_{tot}}$. By replacing (4) in (1) we obtain:

$$R_{tot}=\frac{\pi}{W\cdot\ln\left(\frac{d}{r}\right)}\int_0^L R_{2p}(x)\cdot dx \quad (5)$$

From (5), the factor relating $R_{2p}(x)$ to $R_0(x)$, which we note by **K**, can be calculated by numerically integrating the $R_{2p}(x)$ curve:

$$K=\frac{\ln\left(\frac{d}{r}\right)}{\pi}=\frac{1}{W\cdot R_{tot}}\int_0^L R_{2p}(x)\cdot dx \quad (6)$$

The value obtained for **K** is ~1.867, corresponding to an effective contact radius **r**=4.25μm, in good agreement with the microprobe point radius of ~6 μm measured on the optical microscope.

We can now substitute **K** in formula (4) to obtain the sheet resistance profile:

$$R_0(x)=R_{2p}(x)\cdot\frac{\pi}{\ln\left(\frac{d}{r}\right)}=\frac{R_{2p}(x)}{K}\equiv\frac{R_{2p}(x)}{1.867} \quad (7)$$

For the four probes in line method we use for the sheet resistance the formula given in [15]:

$$R_0(x)=R_{4p}(x)\cdot\frac{\pi}{\ln(2)}\equiv 4.53\cdot R_{4p}(x) \quad (8)$$

where $R_{4p}(x)$ is the 4 probes measured resistance.

From (4) and (8) respectively, the resistivity profile can be calculated by multiplying the sheet resistance with the thickness of the film in each measure point.

4. Results and discussion

4.1 Electrical characteristics

The resistivity profile and the thickness profile of an In_2O_3 film grown at $1.3\text{x}10^{-2}$ mbar oxygen on a 25x12 mm glass substrate with 10 mm wide obstacle, placed at 17 mm from the substrate, is presented in fig. 3. The obstacle size and position on the **x** axis is sketched on the same figure. The film thickness (dashed line) varies from ~800 nm in the non-shadowed regions to ~30 nm in the center of the obstacle shadow. The 2 probes measurement is plotted with solid circles, and the 4 probes measurement is plotted with solid triangles. The spatial interval between the measurement points is 1mm. The scale of the resistivity axis is logarithmic for a better comparison.

In the range 10^{-3} to 10 Ω·cm the 2 and 4 probes methods give identical results. The maximum resistivity, obtained by the 2 probes method in the center of the obstacle shadow, is $\sim 2\text{x}10^{3}$ Ω·cm, and the minimum resistivity, measured with the 4 probes method in the adjacent regions of the film, is $\sim 6\text{x}10^{-4}$ Ω·cm. At low resistivities there is a difference between the values obtained by the two methods (less than 1 order of magnitude) due to the error introduced by the contact resistance in the 2 probes method. The 4 probes method eliminates the contact resistance error by using two probes for injecting current and measuring the voltage on two different probes. In the high resistivity region, the 4 probes method is not accurate, due to the fact that the nanovoltmeter input current becomes comparable with the source compliance current. The compliance current cannot be increased indefinitely, because of the risk of surface leaks on the film.

Separate experiments were performed in order to establish if the variation of the thickness has a role in the variation of the resistivity. In_2O_3 films with thicknesses of 400 and 40 nm (close to the thickness in the obstacle shadow) were grown at the same working pressure of $1.3\text{x}10^{-2}$ mbar oxygen without obstacle [17]. A slight decrease of the resistivity from $\sim 10^{-3}$ to $\sim 6\text{x}10^{-4}$ Ω·cm was observed at the decrease of the thickness, in agreement

with previous studies revealing that the free carriers are generated in the surface and not in the bulk of the oxide thin film [18]. These results prove that the small thickness of the film grown under the obstacle is not responsible for the large increase of the resistivity.

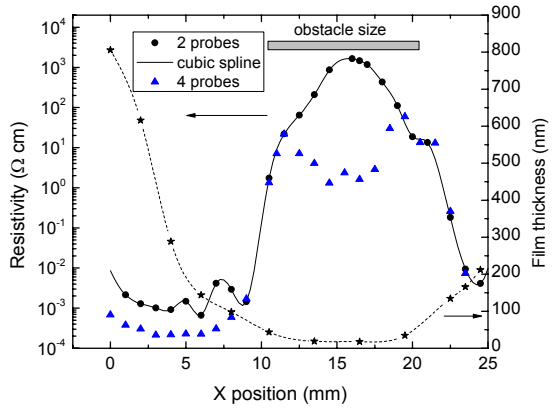

Fig. 3: Resistivity profile in function of the position on the In_2O_3 film (log scale, left axis). The film thickness profile (right axis) is plotted with dashed line and stars. The high resistivity and small thickness values are in the obstacle shadow.

The resistivity variation was explained by analyzing the results of two separate experiments in the absence of the obstacle, at two pressures [17]: at the pressure value used in the above presented experiments ($1.3x10^{-2}$ mbar O_2) and the other at a higher pressure value ($2x10^{-2}$ mbar). The In_2O_3 thin films grown without obstacle at $1.3x10^{-2}$ mbar O_2 on glass are transparent and conducting, having a n-type conduction with resistivity $6x10^{-4}$ Ω·cm, carrier mobility of ~47cm^2/Vs and density of $2.2x10^{20}cm^{-3}$ measured by Hall effect. When the oxygen pressure is increased to $2x10^{-2}$ mbar, the film resistivity reaches up to 10^3 Ω·cm, this means the same resistivity as that of the film grown behind the obstacle at $1.3x10^{-2}$ mbar. The Hall mobility is ~24 cm^2/Vs and the carrier density is $2.5x10^{14}cm^{-3}$. This means that the higher resistivity is mainly due to the decrease of the carrier density. We attribute this decrease to a lower concentration of oxygen vacancies of the films grown at $2x10^{-2}$ mbar O_2 leading to a lower conductivity of these films [1].

Indeed, it has been shown by ^{18}O isotope tracing in PLD [19] that ~30% of the oxygen incorporated in an oxide thin film comes from the ambient gas when the ablation takes place in an oxygen atmosphere at 10^{-2} mbar. When increasing the O_2 pressure to 10^{-1} mbar, the percentage of oxygen incorporated from the ambient gas increases to ~45%. In our case, the oxygen vacancies concentration responsible for conduction in In_2O_3 is significantly reduced by additional incorporation of O_2 from the working gas at higher pressure.

In the case of In_2O_3 films grown with obstacle, the deposition rate of ablated species is reduced by an order of magnitude behind the obstacle, as shown by the film thickness measurements (Fig. 3). Therefore the ratio between the ambient oxygen density and the ablated plasma density increases behind the obstacle as compared to the adjacent regions. This results in more oxygen atoms available per indium atom behind the obstacle, leading to a relative enrichment in oxygen in comparison to the adjacent regions, which explains the resistivity increase in the obstacle shadow [17].

ZnO films were grown without obstacle at different oxygen pressures in order to check the influence of oxygen from the working gas on the film resistivity, like in the case of In_2O_3 films. For a working pressure of $1.3x10^{-2}$ mbar, the Hall and Van der Pauw measurements indicate an n type conduction with a resistivity of $6x10^{-3}$ Ω·cm, carrier mobility ~21 cm^2/Vs and carrier density ~ $5x10^{19}$ cm^{-3}. For a ZnO film grown at $1.5x10^{-2}$ mbar, the value obtained for the resistivity is 0.225 Ω·cm, this means a very close resistivity value to that of the film grown behind the obstacle at $1.3x10^{-2}$ mbar. The carrier density is $9.9x10^{17}$ cm^{-3} and mobility is 28 cm^2/Vs. We notice that the Hall mobility is higher than the one obtained for lower pressure, opposite behavior as compared to In_2O_3 films. The mobility values are comparable, and the carrier density variation is of the same order of magnitude as the resistivity variation. Therefore, the main contribution to the increase of resistivity behind the obstacle remains the$2.5x10^{14}cm^{-3}$. reduction of the carrier density due to the incorporation of oxygen from the working gas, as in the case of In_2O_3 films.

The ZnO thin films were grown with obstacle at $1.3x10^{-2}$ mbar oxygen working pressure. The thickness and resistivity profiles of such a film are presented in figure 4. The thickness of the film varies from 900 nm in the non-shadowed regions to ~100 nm in the obstacle shadow. The resistivity of the ZnO film varies from 0.4 Ω·cm in the obstacle shadow to $6x10^{-3}$ Ω·cm in the adjacent regions. For resistivity measurements only the 2 microprobes method was used, since as shown for the In_2O_3 films, it yields accurate results at resistivities higher than 10^{-3} Ω·cm.

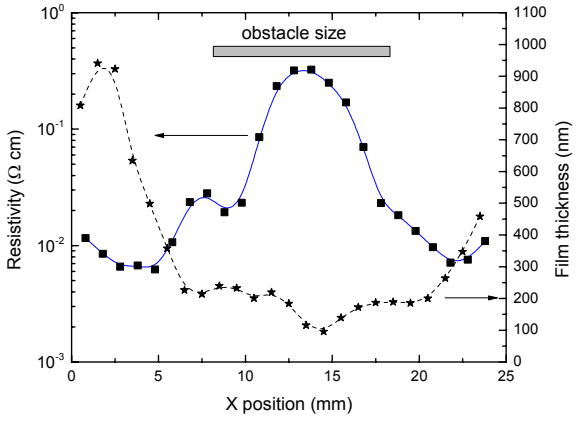

Fig. 4: Resistivity profile in function of the position on the ZnO film (log scale, left axis). The film thickness profile (right axis) is plotted with dashed l ine and stars.

The variation of resistivity is significantly lower (~100 times) than in the case of In_2O_3 film (a factor of 10^6-

10^7). This can be explained by a higher deposition rate of the ZnO film than for the In_2O_3 film in the obstacle shadow as compared to the adjacent region. This leads to a smaller increase of the O/Zn ratio as compared to the O/In ratio behind the obstacle, and in consequence, less additional incorporation of background oxygen in the film behind the obstacle than in the case of In_2O_3.

The higher deposition rate is proved by the greater thickness of the ZnO thin film behind the obstacle (about 100nm) compared to that of the In_2O_3 film (~30nm), for the about the same thickness of 800-900nm in the adjacent regions (Fig 3 and Fig 4). This can be explained by the lower mass of the Zn atoms/ions compared to In atoms/ions (65 vs. 115), leading to a stronger diffusion of Zn ions behind the obstacle compared to In ions [8].

Like in the case of In_2O_3 films, we checked in separate experiments, without obstacle, if the variation of the film thickness plays a role in the variation of the resistivity. The resistivity of a 300 nm ZnO film grown at $1.3x10^{-2}$ mbar without obstacle is $6x10^{-3}$ Ω·cm, equal to the resistivity of the conductive wings in obstacle deposition (fig. 4). For a film grown in the same conditions but with a thickness of 100nm (the same as the thickness in the obstacle shadow), the resistivity increases about 4 times, up to $2.5x10^{-2}$ Ω·cm, opposite situation compared to the In_2O_3 films. This behavior is similar to a metallic film, for which the resistivity increases at very low thickness [20]. This could indicate that the bulk generated carriers have a significant contribution to the conduction of ZnO films grown at low pressure, opposite to In_2O_3 films [18]. However, this increase in resistivity is much smaller than the one observed in the deposition with obstacle (100 times), and this means that the main factor in the increase of the resistivity in the obstacle shadow remains the additional oxygen incorporation behind the obstacle.

4.2 Optical properties

In Fig. 5 a and b the transmittances of the films grown with obstacle are presented, calculated with the total absorption minus the absorption of the optical glass substrate. The substrate itself has a transmittance of 43% at 300 nm wavelength and a cutoff wavelength of 245nm, enough to allow measurements in the near UV. The In_2O_3 film has a high optical transparency (70 – 95% transmittance without substrate) in the visible wavelength range (350-750nm) for the region behind the obstacle, and 40-85% transmittance in the adjacent regions, as it can be seen in figure 5a. The large decrease of the transmittance in the adjacent region for wavelengths higher than 1250 nm is due to the high carrier density of the In_2O_3 film in this region ($2.2x10^{20}cm^{-3}$). Such decrease of the transmittance is not observed in the film region under the obstacle, where the carrier density is much smaller ($2.5x10^{14}cm^{-3}$).

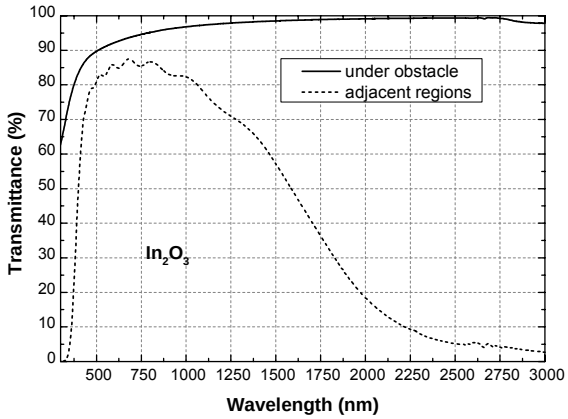

a) In_2O_3 film

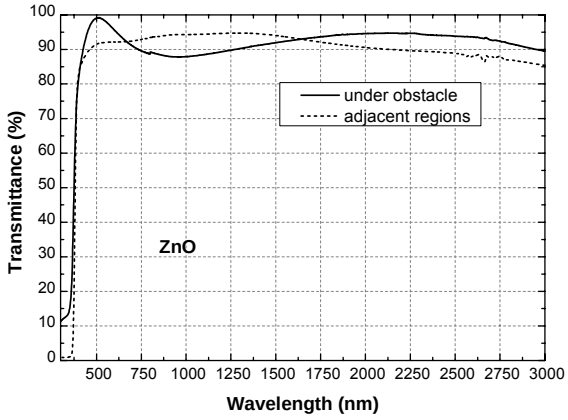

b) ZnO film

Fig. 5. Optical transmittance of the films grown with obstacle (the absorption of the substrate has been compensated). With dotted line, the transmittance of the adjacent film regions (outside the obstacle shadow).

The ZnO film has a transmittance of ~90-98% behind the obstacle and ~90-95% in the adjacent regions, for the same wavelength range (Fig 5b). However, considering the smaller film thickness under the obstacle and the exponential nature of optical absorption, we can conclude that the film grown in the obstacle shadow has a higher optical absorption coefficient than in the adjacent regions. Indeed, the absorption coefficient, whose square value is indirectly shown through the Tauc plot (Fig. 6a and b) is more than 2 times larger in the whole spectral range for the film region behind the obstacle.

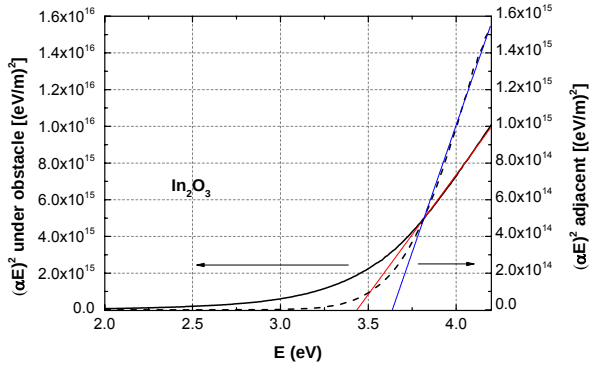

a) In_2O_3 film

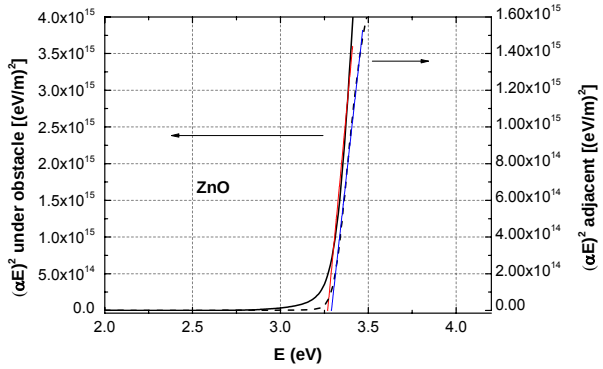

b) ZnO film

Fig. 6. Tauc plot for direct band gap of the films grown behind the obstacle (continuous line, left axis) and outside the obstacle shadow (dashed line, right axis).

The band gap of the In_2O_3 film, obtained by Tauc's plot (Fig. 6a) is ~3.45 eV in the region behind the obstacle and ~3.63 eV in the adjacent regions. Similar values of the band gap for In_2O_3 thin films were reported in previous studies [13, 21]. The Tauc plot of the ZnO thin film (Fig. 6b) indicates a band gap of ~3.27 eV behind the obstacle and ~3.29 eV in the adjacent regions, revealing a smaller influence of the obstacle for these films.

5. Conclusions

In_2O_3 and ZnO thin films grown by PED in the presence of an obstacle exhibit significant differences between the electrical properties of the region grown behind the obstacle and those of the adjacent regions. The ratio ρ_{max}/ρ_{min} between the resistivity of the film region grown in the obstacle shadow and that of the adjacent regions is $\sim 10^7$ for In_2O_3 and $\sim 10^2$ for ZnO, so both films exhibit a considerably higher resistivity in the obstacle shadow region. This fact is explained by the reduction of the deposition rate behind the obstacle, leading to a relatively higher number of oxygen atoms from the working gas available per metal atom in the deposition process behind the obstacle as compared to the adjacent regions, therefore a relative enrichment in oxygen of that film region.

The variation of the carrier mobility measured by Hall effect being small for both ZnO and In_2O_3, the reduction of the free carriers concentration by additional incorporation of background oxygen remains the principal explanation of the increase in resistivity. The smaller dynamics of the resistivity in the case of ZnO could be explained by the lower reduction of the deposition rate in the obstacle shadow for ZnO than for In_2O_3, as shown by the film thickness measurements. The relative enrichment in oxygen in the obstacle shadow is therefore diminished for the ZnO film.

This deposition method could be useful for applications in transparent electronics requiring a single deposition process of a film with both conducting and highly resistive regions, by simply using a shadow mask placed at a certain distance from the substrate. Based on this study, we realized a self-assembled homojunction In_2O_3 transparent thin film transistor (TTFT), by downscaling both the obstacle size and the distance obstacle-substrate by 50 times [17]. The resistivity of the active layer of this TTFT varies from $7x10^5$ Ω·cm in the channel region to 10^{-3} Ω·cm in the source and drain regions.

Acknowledgements

This work was supported by a grant of the Romanian National Authority for Scientific Research, CNCS–UEFISCDI, project number PN-II-ID-PCE-2011-3-0566.

The author is grateful to the cooperative structure around SAFIR (Université Pierre et Marie Curie-Paris 6) for the RBS measurements.

References

[1] J. F. Wager, D. A. Keszler, R. E. Presley, Transparent Electronics (New York: Springer, ISBN 978-0-387-72341-9) 2009
[2] K. Nomura, H. Ohta, A .Takagi, T. Kamiya, H. Hosono Nature **432** 488 (2004).
[3] R. Martins, E. Fortunato, P. Barquinha, L. Pereira Transparent Electronics: From Materials to Devices (New York: Wiley-Blackwell, ISBN 978-0470683736) 2012.
[4] J. Gonzalo, C. N. Alfonso, F. Vega, D. M. Garcia, J. Perrière, Appl. Surf.Sci. **86,** 40 (1995).
[5] E. Millon, M. Nistor, C. Hebert, Y. Davila, J. Perrière J.Mater.Chem **22,** 12179 (2012).
[6] M. Nistor, N. B. Mandache, J. Perrière J. Phys. D: Appl. Phys. **41,** 165205 (2008).
[7] K. Kinoshita, H. Ishibashi, T. Kobayashi Japan.J.Appl.Phys. **33**, L417 (1994).
[8] Z. Trajanovic, S. Choopun, R. P. Sharma, T. Venkatesan Appl. Phys. Lett. **70**, 3461 (1997).
[9] A. Marcu, C. Grigoriu, Jiang W, Yatsui K Thin Solid Films **360**(1-2), 166 (2000).

[10] M. Nistor, A. Ioachim, B. Gallas, D. Defourneau, J. Perrière, W. Seiler J.Phys.Cond. Matt. **19,** 096006 (2007).
[11] M. Nistor, A. Petitmangin, C. Hebert, W. Seiler Appl.Surf.Sci. **257,** 5337 (2011).
[12] S. Tricot, M. Nistor, E. Millon, C. Boulmer-Leborgne, N. B. Mandache, J. Perrière, W. Seiler Surf. Sci**.** **604**(21-22) 2024 (2010).
[13] W. Seiler, M. Nistor, C. Hebert, J. Perrière Solar Energy Materials&Solar Cells **116,** 34 (2013)
[14] M. Nistor, F. Gherendi, N. B. Mandache, IEEE Trans. Plasma Sci. **99,** 2800 (2011).
[15] S. M. Sze, K. Ng. Kwok Physics of Semiconductor Devices, 3rd ed. (John Wiley & Sons ISBN 978-0-471-14323-9) 2006.
[16] J. Rius, S. Manich, R. Rodríguez, M. Ridao, Electrical Characterization of Conductive Ink Layers on Textile Fabrics: Model and Experimental Results, Proceedings of the XXII Conference on Design of Circuits and Integrated Systems (DCIS) – Sevilla (2007), pp.1-6
[17] F. Gherendi, M. Nistor, S. Antohe, L. Ion, I. Enculescu, N. B. Mandache Semicond. Sci. Technol. **28**(8) 085002 (2013). doi: 10.1088/0268-1242/28/8/085002.
[18] S. Lany, A. Zakutayev, T. O. Mason, J. F. Wager, K. R. Poeppelmeier, J. D. Perkins, J. J. Berry, D. S. Ginley, A. Zunger, Phys. Rev. Lett. **108**(1), 2 (2012) doi:10.1103/PhysRevLett.108.016802.
[19] R. Gomez-San Roman, R. Pérez Casero, C. Maréchal, J. P. Enard, J. Perrière, J. Appl. Phys. **80**(3), 1787 (1996).
[20] G. Reiss, E. Hastreiter, H. Brückl, J. Vancea Phys. Rev. B **43**, 5176 (1991).
[21] R. L. Weiher, R. P. Ley, J. Appl. Phys. **37,** 299 (1966).

*Corresponding author: florin.gherendi@infim.ro